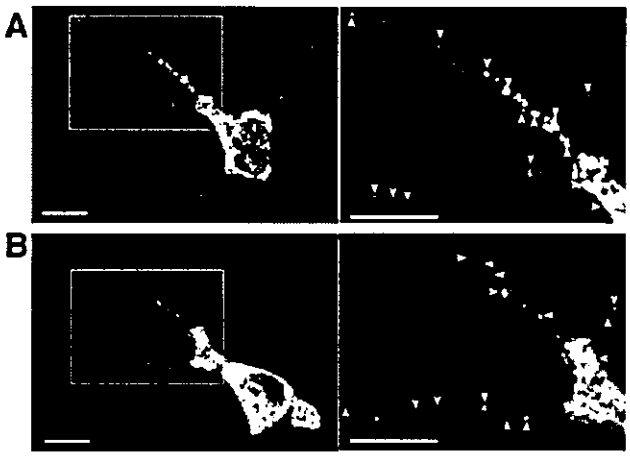

FIG. 3. **The endogenous SYNCRIP protein and expressed GFP-SYNCRIP showed comparable expression patterns in cultured rat hippocampal neurons.** *Right images* are high magnification images of the *boxed region* in the *left images*. *A*, immunolabeling of endogenous SYNCRIP using anti-SYNCRIP-N antibody. *B*, a living cell expressing GFP-SYNCRIP. In both images, many granular structures were observed in dendrites (*arrowheads*). All the images were taken with a confocal microscope. *Scale bars*, 10 μm.

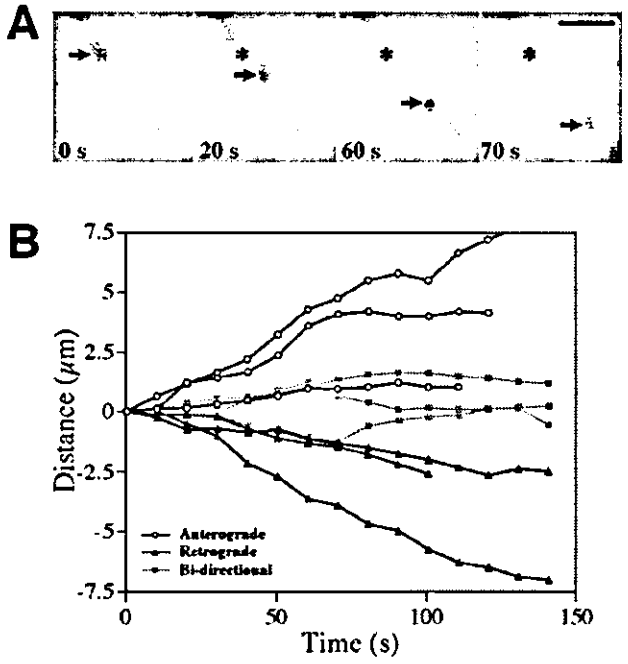

FIG. 4. **Movement of GFP-SYNCRIP-positive granules.** *A*, time-lapse imaging of GFP-SYNCRIP-positive granules in the dendrite recorded with a CCD camera. *Arrows* indicate a moving granule, and *asterisks* indicate the original position of the granule at 0 s. *Scale bar*, 2 μm. *B*, representative movement patterns of GFP-SYNCRIP-positive granules. The net movement of each vesicle (μm) was plotted against time (s). *Anterograde* (positive direction) is the movement from the cell body toward the periphery, and *Retrograde* (negative direction) is the opposite movement. The time-lapse interval was 10 s.

CRIP-positive granules is shown in Fig. 5 (*No drug treatment*). The average velocity of the vesicle movements was about 0.05 μm/s in both the anterograde and retrograde directions as shown in Table I, and the maximum velocity of GFP-SYNCRIP movement was 0.37 μm/s. Interestingly, the speed of SYNCRIP movement was similar to that reported for mRNA granule movement (~0.1 μm/s (9); ~0.1 μm/s (37); 0.03~0.05 μm/s (38)).

The movements of mRNA granules have been reported to be

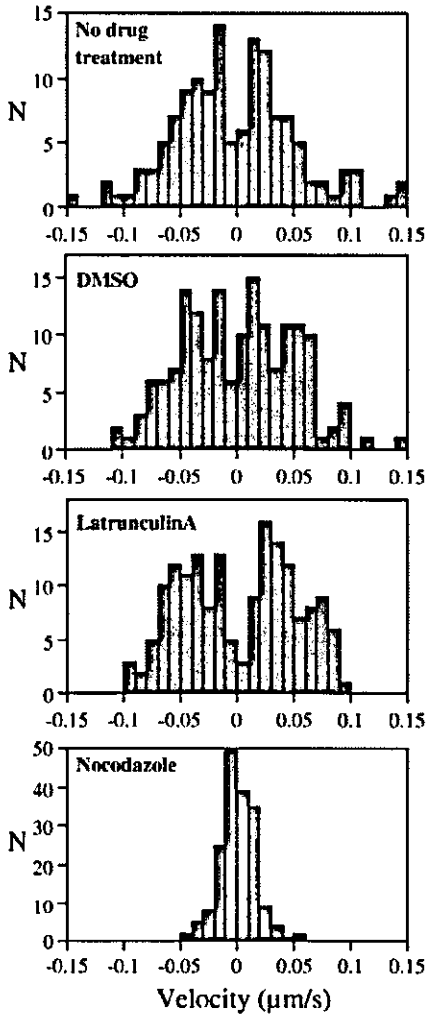

FIG. 5. **Velocity profiles of the GFP-SYNCRIP-positive granules with or without drug treatments.** *N* indicates the number of events, *i.e.* consecutive mono-directional movements. Positive velocity corresponds to the anterograde movement, and negative velocity corresponds to the retrograde movement. *DMSO*, Me_2SO.

mainly dependent on microtubules (9, 18, 35, 37–39). To determine whether microtubules are also involved in the movement of SYNCRIP-positive granules, we tested the effects of drugs that disrupt these cytoskeletal components on the velocity of granule movement. After confirming that these drugs were effective in cultured rat hippocampal neurons by immunocytochemical staining with anti-tubulin antibody (for microtubules) and Alexa 594-phalloidin (for actin filaments) (data not shown), nocodazole (30 μg/ml) and latrunculin A (1 μg/ml) were used to disrupt microtubules and actin filaments, respectively. Neither substance had a major effect on the distribution pattern or number of granules labeled with GFP-SYNCRIP. Latrunculin A did not have a significant effect on the velocity of GFP-SYNCRIP-positive granules in comparison with control cells exposed to 0.3% Me_2SO ($p > 0.1$, *t* test, and Mann-Whitney *U* test). However, nocodazole significantly decreased the velocity of GFP-SYNCRIP-positive granules by ~70% in both directions compared with control cells ($p < 0.001$, *t* test and Mann-Whitney *U* test, Fig. 5 and Table I). These results suggest that the transport of SYNCRIP-positive granules is highly dependent on microtubules and that the contribution of the actin cytoskeleton is minor, which is consistent with previous reports for the transport of mRNA granules.

TABLE 1
Effects of drug treatment on the velocity of the movement of GFP-SYNCRIP-positive granules

Drug	Anterograde	Retrograde
	μm/s	*μm/s*
No drug treatment	0.050 ± 0.051 (n = 66)[a]	0.055 ± 0.058 (n = 75)
Me_2SO	0.041 ± 0.028 (n = 84)	0.041 ± 0.025 (n = 79)
Latrunculin A	0.045 ± 0.023 (n = 85)	0.043 ± 0.023 (n = 82)
Nocodazole	0.014 ± 0.010 (n = 90)[b]	0.012 ± 0.009 (n = 89)[b]

[a] Values show average ± S.D.
[b] $p < 0.001$ (t test, Mann-Whitney U test)

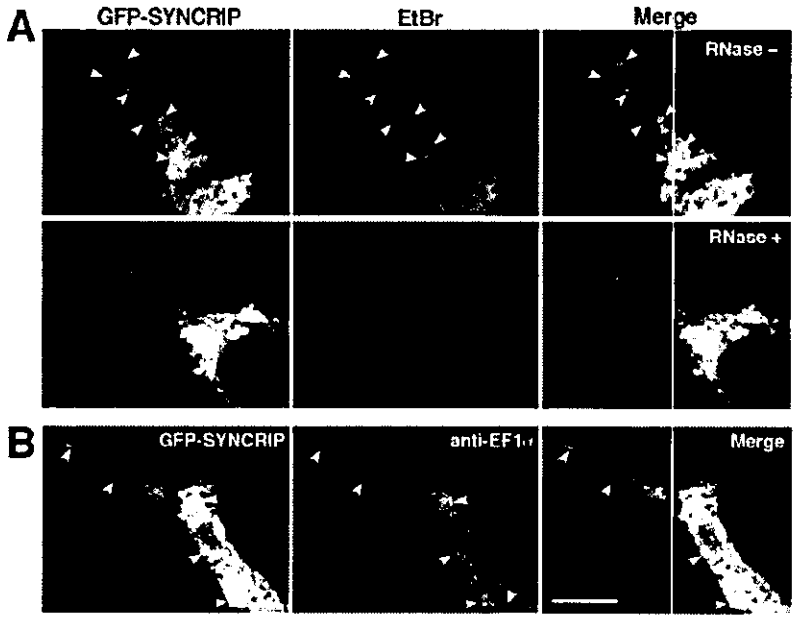

FIG. 6. **The GFP-SYNCRIP protein co-localized with the components of mRNA granules.** *A*, RNA labeling of GFP-SYNCRIP-expressing neurons with EtBr. *Top*, EtBr signals overlapped with GFP-SYNCRIP-positive granules (*arrowheads*). *Bottom*, EtBr signals were abolished by treatment with RNase A. *B*, double-labeling with GFP-SYNCRIP and endogenous EF1α, a marker for mRNA granules. Endogenous EF1α was found on the GFP-SYNCRIP-labeled granules (*arrowheads*). Images were taken with a confocal microscope. The *scale bar* indicates 10 μm.

SYNCRIP Was Co-localized with Dendritic RNAs and Markers of mRNA Granules—We then investigated whether the distribution of SYNCRIP overlaps with that of RNA and mRNA granule markers in dendrites of cultured hippocampal neurons. Dendritic RNAs were labeled with EtBr as described previously (35). The EtBr signal was completely abolished by RNase treatment, indicating that it was specific for RNA (Fig. 6*A*, *bottom*). In the absence of RNase, EtBr labeled granular structures in the cell bodies and dendrites, which overlapped with the most of the SYNCRIP-positive granules (Fig. 6*A*, *top*).

We also investigated whether GFP-SYNCRIP was co-localized with protein components of mRNA granules, *i.e.* EF1α (9) and staufen (15, 40). Immunocytochemistry using anti-EF1α antibody revealed that GFP-SYNCRIP-positive granules were co-localized with endogenous EF1α (Fig. 6*B*). However, we were not able to perform immunocytochemistry for staufen, because no specific antibody against rat staufen was available. Instead, we used GFP-tagged human staufen1 (GFP-hStau1), which is transported within dendrites as a component of mRNA granules (37). GFP-hStau1 was co-expressed with SYNCRIP tagged with monomeric RFP (mRFP-SYCNRIP), whose behavior was indistinguishable from that of GFP-SYNCRIP (data not shown). mRFP-SYNCRIP was co-localized with GFP-hStau1 in granules (Fig. 7*A*), and we confirmed that the GFP-hStau1-positive granules contained endogenous SYNCRIP by immunocytochemistry (supplemental data S1). These results strongly indicate that SYNCRIP is a component of the mRNA granule in neurons.

SYNCRIP Is a Component of Moving mRNA Granules Containing the 3′-UTR of IP_3R1 mRNA—Fig. 7*B* and supplemental Movie 2 show representative time-lapse images of a dendrite from a hippocampal neuron expressing mRFP-SYNCRIP and GFP-hStau1. The mRFP-SYNCRIP signal completely overlapped with that of GFP-hStau1 throughout the movement, indicating that SYNCRIP is a component of the "moving" mRNA granules.

Finally, we investigated whether the SYNCRIP-positive granules actually transport meaningful sets of mRNAs. The mRNA of IP_3R1 is expressed in central nervous system neurons, including hippocampal neurons (41). In addition, IP_3R1 mRNA has been shown to be present in the dendrites of cerebellar Purkinje cells and neocortical neurons (41, 42). Because a sequence homologous to the hnRNP A2 response element (A2RE, GCCAAGGAGCCAGAGAGCATG), which is included in a subset of dendritically localized mRNAs generally transported as components of mRNA granules (18, 43), is found in the 3′-UTR of IP_3R1 mRNA (GCAAATGAGGCAGAGGGACTC, bases identical to those of A2RE are underlined), it is a candidate for a component of mRNA granules. We visualized the 3′-UTR of IP_3R1 mRNA in living neurons by a GFP-based mRNA labeling technique that was first reported in yeast (29) and was used later to visualize several mRNAs in neuronal dendrites (17, 38). We prepared two plasmids, with one (NLS-MS2-Venus) containing the coding sequences of the single-stranded RNA phage capsid protein MS2 fused with Venus (a brighter variant of yellow fluorescent protein (30)) and an NLS. The other plasmid (IP_3R1 3′-UTR-MS2bs) contained 12 repeats of the MS2 binding sequence, each of which encoded a 17-nucleotide RNA stem loop fused with the 3′-UTR of IP_3R1 mRNA (bases 8579–9041). When these plasmids were co-transfected into hippocampal neurons, small bright granules were seen in the dendrites (Fig. 8*A*, *top*), whereas diffuse, not punctate staining was seen in the dendrites in a control experiment in which NLS-MS2-Venus alone was transfected (Fig. 8*A*, *bot-*

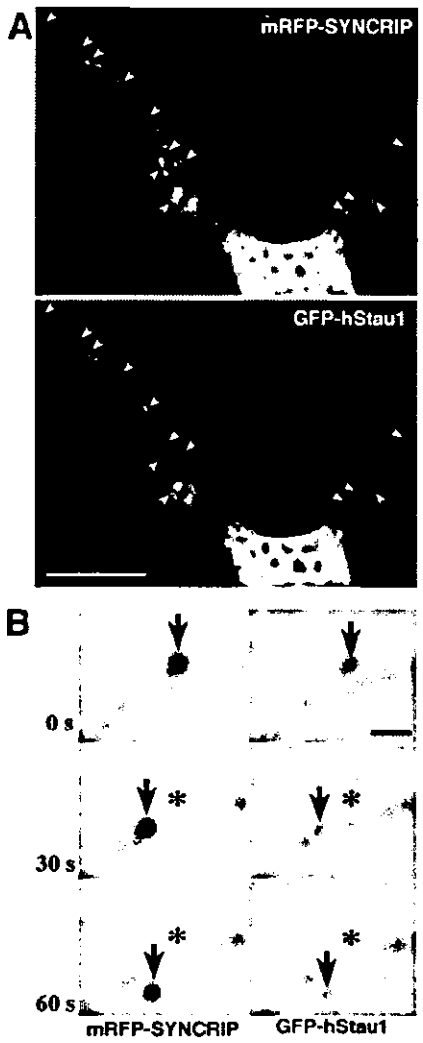

FIG. 7. **mRFP-SYNCRIP proteins were incorporated in motile mRNA granules.** *A*, double labeling of neurons with mRFP-SYNCRIP and GFP-tagged human staufen (GFP-hStau1). mRFP-SYNCRIP and GFP-hStau1 co-localized on the same granules (*arrowheads*). Images were taken with a confocal microscope. *Scale bar*, 10 μm. *B*, time-lapse images of a granule containing mRFP-SYNCRIP and GFP-hStau1 in a dendrite. *Left*, consecutive frames showing a mRFP-SYNCRIP signal. *Right*, corresponding frames showing a GFP-hStau1 signal. *Arrows* indicate a moving granule, and *asterisks* indicate the original position of the granule at 0 s. Note that both mRFP-SYNCRIP and GFP-hStau1 labeled the same moving granule. *Scale bar*, 2 μm.

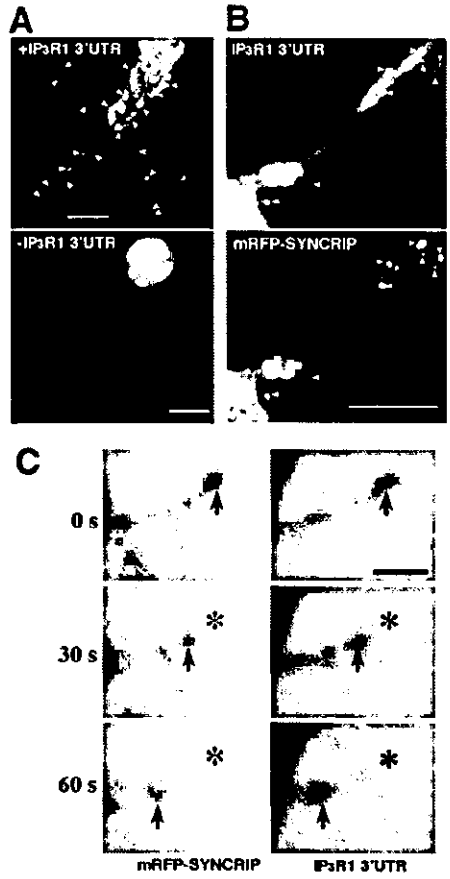

FIG. 8. **3′-UTR of IP_3R1 mRNA was co-transported with mRFP-SYNCRIP.** *A*, to visualize the 3′-UTR of IP_3R1 mRNA, cultured neurons were co-transfected with plasmid DNAs encoding 3′-UTR of mouse IP_3R1 mRNA fused with 12 copies of the MS2 binding sequence (IP_3R1 3′-UTR-MS2bs) and Venus fused with the MS2 and NLS (NLS-MS2-Venus). IP_3R1 3′-UTR mRNAs expressed in neurons was distributed as granular structures (*top*, *arrowheads*). On the other hand, a diffuse staining pattern was observed when NLS-MS2-Venus alone was transfected (*bottom*). *B*, double labeling of cultured neurons with 3′-UTR of IP_3R1 mRNA and mRFP-SYNCRIP. Many of the Venus-positive granules were mRFP-SYNCRIP-positive (*arrowheads*). Images in *A* and *B* were taken with a confocal microscope. *Scale bars*, 10 μm. *C*, movement of a granule containing mRFP-SYNCRIP and 3′-UTR of IP_3R1 mRNA in a dendrite. *Left*, consecutive frames showing a mRFP-SYNCRIP signal. *Right*, corresponding frames showing a 3′-UTR of IP_3R1 mRNA signal detected by Venus. A CCD camera was used. *Arrows* indicate a moving granule, and *asterisks* indicate the original position of the granule at 0 s. Note that both mRFP-SYNCRIP and the 3′-UTR of IP_3R1 mRNA were on the same moving granule. *Scale bar*, 2 μm.

tom). These granules were also labeled with mRFP-SYNCRIP when mRFP-SYNCRIP was further added to the co-transfected plasmids (Fig. 8*B*). A multicolor time-lapse study revealed that the movement of the IP_3R1 3′-UTR mRNA signal coincided with that of the mRFP-SYNCRIP (Fig. 8*C* and supplemental Movie 3). Taken together, these findings indicate that SYNCRIP is a component of mRNA granules that at least transports IP_3R1 mRNA.

DISCUSSION

In the proteomics study we showed that the SYNCRIP-associated complexes in 293EBNA cells contain at least 111 proteins, some of which seem to be responsible for mRNA processing and translation (Fig. 1 and supplemental Table SI). Cytoplasmic ribosomal proteins and RNA binding proteins such as hnRNP A2/B1, zip code-binding protein 1 (IGF-II mRNA-binding protein 1), and hnRNP U, which are the components of mRNA granules (17, 18, 44), were also detected as major SYNCRIP-associated proteins, and this fact raised the possibility that SYNCRIP plays roles as a component of mRNA granules in the neurons. Very recently, a screening study for RNase-sensitive granules that associate with motor protein kinesin revealed that SYNCRIP is one of the components of mRNA transporting granule (44). Moreover, proteomic and immunoelectron microscopic analyses showed that SYNCRIP is included in mRNA granules purified from rat brains.[2] Our new lines of evidence further strengthen these reports that SYNCRIP is a component of mRNA granules. SYNCRIP were distributed in dendrites of hippocampal neurons as a granular structure (Figs. 2 and 3), and the SYNCRIP-containing granules were transported bi-directionally at a speed of ~0.05 μm/s in a microtubule-dependent manner (Fig. 4 and Table I), as was

[2] W. S. Sossin and P. S. McPherson, Montreal Neurological Institute, McGill University, Quebec, Canada, personal communication.

previously reported for mRNA granule dynamics (9, 18, 35, 37–39, 44). SYNCRIP in the dendrite co-localized with RNA and the component of mRNA granules (Figs. 5–7) and was co-transported with IP_3R1 mRNA (Fig. 8). The molecular mechanism underlying the recruitment of SYNCRIP into mRNA granules remains unknown. One possibility is that SYNCRIP interacts with poly(A) or AU-rich regions that are generally present in the 3′ region of mRNAs, as was supported by the fact that SYNCRIP interacts directly with poly(A) and poly(U) *in vitro* (19, 22, 23). Another possibility is that SYNCRIP is bound to mRNA granules as a component of a protein complex as is reported for a human homolog of SYNCRIP in a non-neuronal cell (24). Clarification of the binding relations among the components of mRNA granules may be required to investigate these possibilities.

It is interesting that a number of mitochondrial ribosomal proteins associated with SYNCRIP in 293EBNA cells (Fig. 1 and supplemental Table SI). However, SYNCRIP was not found in mitochondria either in the human kidney cell line and the cultured hippocampal neuron (data not shown). SYNCRIP might associate with mitochondrial ribosomal proteins in the cytoplasm and have indirect roles in protein synthesis in mitochondria, but further study is required to test this possibility.

Microtubule-based motor proteins kinesin and dynein are possibly responsible for the transport of SYCNRIP-positive mRNA granule, since they were co-purified with SYNCRIP-containing mRNA granules (44).[2] mRNA granules that contain cytoplasmic polyadenylation element-binding protein has also been shown to be co-localized with molecular motor kinesin and dynein (39). Bi-directional movement of GFP-SYNCRIP-positive granules (Fig. 4) could be explained by mixed polarity of the dendritic microtubules (45) or by coordination of multiple, opposite-directed motor proteins. In the present study, actin filaments were shown to contribute little to the transport of SYNCRIP (Fig. 5 and Table I), which has also been reported to be the case for the movement of hnRNP A2-positive mRNA granules (18). Although actin filaments seem less involved in the transport of mRNA granules, an actin motor myosin V is shown to be a component of the mRNA/protein complex containing staufen and fragile X mental retardation protein (46). Our results do not necessarily exclude a possible association of SYNCRIP-containing mRNA granules with actin filaments.

The speed of GFP-SYNCRIP-positive granule movement (~0.05 μm/s, Fig. 5) was comparable with that of mRNA granules visualized by SYTO14 (0.1 μm/s, 9), of staufen-containing granules (~0.1 μm/s, 37), and of mRNA granules containing the 3′-UTR of CaMKIIα mRNA (0.03~0.05 μm/s (38)). However, the speed of GFP-SYNCRIP was much slower than that of zip code-binding protein 1 and β-actin mRNA-positive granules, which move at an average velocity of ~1.0 μm/s (17), which exceeds the maximum speed of GFP-SYNCRIP movement (0.37 μm/s). This result suggests a possibility that SYNCRIP is not involved in mRNA granules that are transported at a fast speed. Variety in the transport speeds of mRNA granules may reflect the heterogeneity in mRNA granules that has been proposed recently (47).[2] In addition to the differences in the motor proteins interacting with each subset of mRNA granules, interaction between mRNA granules and organelles may modulate the dynamics of mRNA granules. mRNA granules containing staufen and fragile X mental retardation protein are reported to associate with rough endoplasmic reticulum (46), and this association may affect the transport of mRNA granules. Further work is required to understand the heterogeneity in mRNA granules and their transport.

In this study, we have demonstrated that 3′-UTR of IP_3R1 is co-transported with SYNCRIP as mRNA granules (Fig. 8). Although IP_3R1 mRNA was previously shown to be present in the dendrites of cerebellar Purkinje cells and neocortical neurons (41, 42), the mechanism underlying the dendritic distribution of IP_3R1 mRNA has never been elucidated. This study suggests that IP_3R1 mRNA may be delivered into the dendrites via mRNA granule transport and that 3′-UTR of IP_3R1 mRNA may contain a targeting signal to dendritic mRNA granules, as is known for other dendritic localized mRNAs. IP_3R plays an important role, such as induction of synaptic plasticity in neuronal dendrites (48–50). The dendritic localization and local translation of CaMKIIα mRNA are responsible for the delivery of the kinase and for the induction of synaptic plasticity (51). The dendritic transported mRNA granules containing IP_3R1 mRNA may also be important for accurate delivery of IP_3R1 proteins into the post-synapse and for the induction of synaptic plasticity.

Although the physiological roles of SYNCRIP are still poorly understood even in non-neuronal cells, some interesting properties of SYNCRIP have been reported. Because SYNCRIP is a component of a protein complex that stabilizes c-*fos* mRNA (24), it is possible that SYNCRIP also stabilizes mRNAs during their transport in dendrites. Insulin stimulation and osmotic shocks are reported to induce phosphorylation of tyrosine residues of SYNCRIP, and the RNA binding activity of SYNCRIP is modified by phosphorylation (22, 23). Insulin is present in the brain (for review, see Ref. 52), and insulin receptor tyrosine kinases are abundant in the hippocampus, especially in neuronal dendrites, including synapses (53, 54). In addition, overexpressed fibroblast growth factor receptor 1, a receptor tyrosine kinase that is expressed in hippocampal neurons (55), is also shown to phosphorylate a human homolog of SYNCRIP (NSAP1) on its tyrosine 373, which is located in the third RNA recognition motif domain (56). These studies raise intriguing possibilities that the turnover or translation of mRNAs contained within mRNA granules could be controlled by the insulin- or fibroblast growth factor-dependent phosphorylation of SYNCRIP in hippocampal neurons. Elucidating the functions of SYNCRIP and its regulatory mechanism in mRNA granules may provide an important key for understanding the temporal and spatial regulation of the local translation of mRNA involved in the induction of synaptic plasticity.

Acknowledgments—We thank Dr. R. Tsien (University of California, San Diego, CA) for the gift of monomeric RFP, Dr. S. Sugano (The Institute of Medical Science, The University of Tokyo, Tokyo, Japan) for the gift of a cDNA clone for human staufen1 (HEP22160), Dr. R. Singer (Saint Mary's University, Nova Scotia, Canada) for the gift of pGA14-MS2-GFP, Dr. A. Miyawaki (RIKEN, Saitama, Japan) for the gift of CS2-Venus, and Drs. McPherson and Sossin (Montreal Neurological Institute, McGill University, Quebec, Canada) for valuable discussions. We also thank M. Iwai (The University of Tokyo) for assistance with plasmid construction.

REFERENCES

1. Bashirullah, A., Cooperstock, R. L., and Lipshitz, H. D. (1998) *Annu. Rev. Biochem.* **67**, 335–394
2. Kuhl, D., and Skehel, P. (1998) *Curr. Opin. Neurobiol.* **8**, 600–606
3. Tiedge, H., Bloom, F. E., and Richter, D. (1999) *Science* **283**, 186–187
4. Kiebler, M. A., and DesGroseillers, L. (2000) *Neuron* **25**, 19–28
5. Kacharmina, J. E., Job, C., Crino, P., and Eberwine, J. (2000) *Proc. Natl. Acad. Sci. U. S. A.* **97**, 11545–11550
6. Aakalu, G., Smith, W. B., Nguyen, N., Jiang, C., and Schuman, E. M. (2001) *Neuron* **30**, 489–502
7. Job, C., and Eberwine, J. (2001) *Proc. Natl. Acad. Sci. U. S. A.* **98**, 13037–13042
8. Steward, O., and Schuman, E. M. (2003) *Neuron* **40**, 347–359
9. Knowles, R. B., Sabry, J. H., Martone, M. E., Deerinck, T. J., Ellisman, M. H., Bassell, G. J., and Kosik, K. S. (1996) *J. Neurosci.* **16**, 7812–7820
10. Racca, C., Gardiol, A., and Triller, A. (1997) *J. Neurosci.* **17**, 1691–1700
11. Wanner, I., Baader, S. L., Brich, M., Oberdick, J., and Schilling, K. (1997) *Histochem. Cell Biol.* **108**, 345–357
12. Tiedge, H., and Brosius, J. (1996) *J. Neurosci.* **16**, 7171–7181
13. Torre, E. R., and Steward, O. (1996) *J. Neurosci.* **16**, 5967–5978
14. Feng, Y., Gutekunst, C. A., Eberhart, D. E., Yi, H., Warren, S. T., and Hersch, S. M. (1997) *J. Neurosci.* **17**, 1539–1547
15. Kiebler, M. A., Hemraj, I., Verkade, P., Köhrmann, M., Fortes, P., Marion, R. M., Ortin, J., and Dotti, C. G. (1999) *J. Neurosci.* **19**, 288–297

16. Severt, W. L., Biber, T. U., Wu, X., Hecht, N. B., DeLorenzo, R. J., and Jakoi, E. R. (1999) *J. Cell Sci.* **112,** 3691–3702
17. Tiruchinapalli, D. M., Oleynikov, Y., Kelic, S., Shenoy, S. M., Hartley, A., Stanton, P. K., Singer, R. H., and Bassell, G. J. (2003) *J. Neurosci.* **23,** 3251–3261
18. Shan, J., Munro, T. P., Barbarese, E., Carson, J. H., and Smith, R. (2003) *J. Neurosci.* **23,** 8859–8866
19. Mizutani, A., Fukuda, M., Ibata, K., Shiraishi, Y., and Mikoshiba, K. (2000) *J. Biol. Chem.* **275,** 9823–9831
20. Harris, C. E., Boden, R. A., and Astell, C. R. (1999) *J. Virol.* **73,** 72–80
21. Mourelatos, Z., Abel, L., Yong, J., Kataoka, N., and Dreyfuss, G. (2001) *EMBO J.* **20,** 5443–5452
22. Hresko, R. C., and Mueckler, M. (2000) *J. Biol. Chem.* **275,** 18114–18120
23. Hresko, R. C., and Mueckler, M. (2002) *J. Biol. Chem.* **277,** 25233–25238
24. Grosset, C., Chen, C. Y., Xu, N., Sonenberg, N., Jacquemin-Sablon, H., and Shyu, A. B. (2000) *Cell* **103,** 29–40
25. Yanagida, M., Shimamoto, A., Nishikawa, K., Furuichi, Y., Isobe, T., and Takahashi, N. (2001) *Proteomics* **1,** 1390–1404
26. Natsume, T., Yamauchi, Y., Nakayama, H., Shinkawa, T., Yanagida, M., Takahashi, N., and Isobe, T. (2002) *Anal. Chem.* **74,** 4725–4733
27. Yanagida, M., Hayano, T., Yamauchi, Y., Shinkawa, T., Natsume, T., Isobe, T., and Takahashi, N. (2004) *J. Biol. Chem.* **279,** 1607–1614
28. Campbell, R. E., Tour, O., Palmer, A. E., Steinbach, P. A., Baird, G. S., Zacharias, D. A., and Tsien, R. Y. (2002) *Proc. Natl. Acad. Sci. U. S. A.* **99,** 7877–7882
29. Bertrand, E., Chartrand, P., Schaefer, M., Shenoy, S. M., Singer, R. H., and Long, R. M. (1998) *Mol. Cell* **2,** 437–445
30. Nagai, T., Ibata, K., Park, E. S., Kubota, M., Mikoshiba, K., and Miyawaki, A. (2002) *Nat. Biotechnol.* **20,** 87–90
31. Higgins, D., and Banker, G. (1998) in *Culturing Nerve Cells* (Banker, G., and Goslin, K., eds) pp. 37–78, MIT Press, Cambridge, MA
32. Bannai, H., Inoue, T., Nakayama, T., Hattori, M., and Mikoshiba, K. (2004) *J. Cell Sci.* **117,** 163–175
33. Köhrmann, M., Haubensak, W., Hemraj, I., Kaether, C., Leßmann, V. J., and Kiebler, M. A. (1999) *J. Neurosci. Res.* **58,** 831–835
34. Blanpied, T. A., Scott, D. B., and Ehlers, M. D. (2002) *Neuron* **36,** 435–449
35. Tang, S. J., Meulemans, D., Vazquez, L., Colaco, N., and Schuman, E. (2001) *Neuron* **32,** 463–475
36. O'Brien, T. W. (2002) *Gene (Amst.)* **286,** 73–79
37. Köhrmann, M., Luo, M., Kaether, C., DesGroseillers, L., Dotti, C. G., and Kiebler, M. A. (1999) *Mol. Biol. Cell* **10,** 2945–2953
38. Rook, M. S., Lu, M., and Kosik, K. S. (2000) *J. Neurosci.* **20,** 6385–6393
39. Huang, Y. S., Carson, J. H., Barbarese, E., and Richter, J. D. (2003) *Genes Dev.* **17,** 638–653
40. Mallardo, M., Deitinghoff, A., Muller, J., Goetze, B., Macchi, P., Peters, C., and Kiebler, M. A. (2003) *Proc. Natl. Acad. Sci. U. S. A.* **100,** 2100–2105
41. Furuichi, T., Simon-Chazottes, D., Fujino, I., Yamada, N., Hasegawa, M., Miyawaki, A., Yoshikawa, S., Guenet, J. L., and Mikoshiba, K. (1993) *Receptors Channels* **1,** 11–24
42. Bagni, C., Mannucci, L., Dotti, C. G., and Amaldi, F. (2000) *J. Neurosci.* **20,** 1–6
43. Ainger, K., Avossa, D., Diana, A. S., Barry, C., Barbarese, E., and Carson, J. H. (1997) *J. Cell Biol.* **138,** 1077–1087
44. Kanai, Y., Dohmae, N., and Hirokawa, N. (2004) *Neuron* **43,** 513–525
45. Baas, P. W., Deitch, J. S., Black, M. M., and Banker, G. A. (1988) *Proc. Natl. Acad. Sci. U. S. A.* **85,** 8335–8339
46. Ohashi, S., Koike, K., Omori, A., Ichinose, S., Ohara, S., Kobayashi, S., Sato, T. A., and Anzai, K. (2002) *J. Biol. Chem.* **277,** 37804–37810
47. Duchaine, T. F., Hemraj, I., Furic, L., Deitinghoff, A., Kiebler, M. A., and DesGroseillers, L. (2002) *J. Cell Sci.* **115,** 3285–3295
48. Inoue, T., Kato, K., Kohda, K., and Mikoshiba, K. (1998) *J. Neurosci.* **18,** 5366–5373
49. Fujii, S., Matsumoto, M., Igarashi, K., Kato, H., and Mikoshiba, K. (2000) *Learn. Mem.* **7,** 312–320
50. Nishiyama, M., Hong, K., Mikoshiba, K., Poo, M. M., and Kato, K. (2000) *Nature* **408,** 584–588
51. Miller, S., Yasuda, M., Coats, J. K., Jones, Y., Martone, M. E., and Mayford, M. (2002) *Neuron* **36,** 507–519
52. Wozniak, M., Rydzewski, B., Baker, S. P., and Raizada, M. K. (1993) *Neurochem. Int.* **22,** 1–10
53. Hill, J. M., Lesniak, M. A., Pert, C. B., and Roth, J. (1986) *Neuroscience* **17,** 1127–1138
54. Abbott, M. A., Wells, D. G., and Fallon, J. R. (1999) *J. Neurosci.* **19,** 7300–7308
55. Lin, S. D., and Fann, M. J. (1998) *J. Biomed. Sci.* **5,** 111–119
56. Hinsby, A. M., Olsen, J. V., Bennett, K. L., and Mann, M. (2003) *Mol. Cell. Proteomics* **2,** 29–36

THE JOURNAL OF BIOLOGICAL CHEMISTRY
Vol. 279, No. 47, Issue of November 19, pp. 48976–48982, 2004
Printed in U.S.A.

Lateral Diffusion of Inositol 1,4,5-Trisphosphate Receptor Type 1 Is Regulated by Actin Filaments and 4.1N in Neuronal Dendrites*

Received for publication, July 23, 2004, and in revised form, September 9, 2004
Published, JBC Papers in Press, September 10, 2004, DOI 10.1074/jbc.M408364200

Kazumi Fukatsu‡, Hiroko Bannai‡§, Songbai Zhang¶, Hideki Nakamura‡, Takafumi Inoue‡¶, and Katsuhiko Mikoshiba‡§¶‡‡**

From the ‡Division of Molecular Neurobiology and ‡‡Division of Neural Signal Information Nippon Telegraph and Telephone Company-The Institute of Medical Science, The University of Tokyo, 4-6-1 Shirokanedai, Minato-ku, Tokyo 108-8639, Japan, the §Laboratory for Developmental Neurobiology, Brain Science Institute, RIKEN, 2-1 Hirosawa, Wako, Saitama 351-0198, Japan, the ¶Calcium Oscillation Project, ICORP, Japan Science and Technology Corporation, 3-4-4 Shirokanedai, Minato-ku, Tokyo 108-0071, Japan, and the ‖Department of Physics, Graduate School of Science, The University of Tokyo, 7-3-1 Hongo, Bunkyo-ku, Tokyo 113-0033, Japan

Inositol 1,4,5-trisphosphate receptor type1 (IP_3R1) plays an important role in neuronal functions; however, the lateral diffusion of IP_3R1 on the endoplasmic reticulum membrane and its regulation in the living neurons remain unknown. We expressed green fluorescent protein-tagged IP_3R1 in cultured rat hippocampal neurons and observed the lateral diffusion by the fluorescence recovery after photobleaching technique. IP_3R1 showed lateral diffusion with an effective diffusion constant of ~0.3 $\mu m^2/s$. Depletion of actin filaments increased the diffusion constant of IP_3R1, suggesting that the diffusion of IP_3R1 is regulated negatively through actin filaments. We also found that protein 4.1N, which binds to IP_3R1 and contains an actin-spectrin-binding region, was responsible for this actin regulation of the IP_3R1 diffusion constant. Overexpression of dominant-negative 4.1N and blockade of 4.1N binding to IP_3R1 increased the IP_3R1 diffusion constant. The diffusion of IP_3R type 3 (IP_3R3), one of the isoforms of IP_3Rs lacking the binding ability to 4.1N, was not dependent on actin filaments but became dependent on actin filaments after the addition of a 4.1N-binding sequence. These data suggest that 4.1N serves as a linker protein between IP_3R1 and actin filaments. This actin filament-dependent regulation of IP_3R1 diffusion may be important for the spatiotemporal regulation of intracellular Ca^{2+} signaling.

Inositol 1,4,5-trisphosphate (IP_3)[1] receptors (IP_3Rs) are intracellular Ca^{2+} channels that are responsible for Ca^{2-} release from intracellular stores (1) and located on the membrane of the endoplasmic reticulum (ER). IP_3, which is generated in response to various extracellular stimuli, binds to IP_3Rs and induces Ca^{2+} release (IP_3-induced Ca^{2+} release; IICR) (1, 2). IICR plays crucial roles in various neuronal activities. For example, mouse strains mutated in the IP_3R type 1 (IP_3R1) gene display severe ataxia and epileptic seizures (3, 4). The control of nerve growth in chick dorsal root ganglia neurons is dependent on IP_3R1 (5). IICR is also known to be involved in long term potentiation and long term depression in the hippocampal CA1 area (6, 7) and in long term depression in cerebellar Purkinje cells (8). Interestingly, IICR in neurons is highly restricted spatially (9, 10), although the ER is spread throughout the cell, and the induction of synaptic plasticity (11) and regulation of nerve growth (5) require spatially restricted IICR. Some ER Ca^{2-}-handling proteins including IP_3Rs show uneven distribution patterns (12), and this heterogeneity is postulated to be responsible for the spatially and temporally heterogeneous Ca^{2+} signaling patterns. Thus, targeting of IP_3Rs to specific regions in the cell may be one of the important factors in the spatial regulation of IICR; however, the molecular mechanisms underlying the spatial regulation of IICR remain to be elucidated.

The dynamics of the α-amino-3-hydroxy-5-methyl-4-isoxazole-propionic acid (AMPA) type glutamate receptor (AMPAR) have been intensively studied. In addition to an elaborate mechanism for insertion and removal from the plasma membrane (13), the lateral diffusion of AMPAR on the plasma membrane is regulated actively, especially by local Ca^{2+} signals (14, 15). All of the dynamics of AMPAR have been implied to play important roles in the regulation of synaptic transmission and plasticity. Thus, the distribution pattern of IP_3Rs and their dynamics in dendrites is also considered to be important for the fine tuning of Ca^{2+}-dependent events, such as synaptic plasticity, that are little understood to date.

We have shown the existence of vesicular ERs that are transported along dendrites bi-directionally with a fast velocity (0.2–0.3 μm/s) (16), in addition to the ER in reticular structure. In this study, we focused on the dynamics of ER membrane proteins in the reticular ER in dendrites of cultured hippocampal neurons and observed their diffusive movements using the fluorescence recovery after photobleaching (FRAP) technique. To our surprise, the diffusive movement of IP_3R1 was regulated through actin filaments, and this regulation was not seen for other ER membrane proteins such as sarcoplasmic/endoplasmic reticulum calcium-ATPase (SERCA) and IP_3R type 3 (IP_3R3). Furthermore, we found that the actin-spectrin-binding

* This work was supported by grants from the Ministry of Education, Culture, Sports, Science and Technology of Japan (to T. I. and K. M.), the Ministry of Health, Labour and Welfare of Japan (to T. I.), and the 21st Century COE Program, Center for Integrated Brain Medical Science, from the Ministry of Education, Culture, Sports, Science and Technology of Japan (to K. F. and H. N.). The costs of publication of this article were defrayed in part by the payment of page charges. This article must therefore be hereby marked "*advertisement*" in accordance with 18 U.S.C. Section 1734 solely to indicate this fact.

** To whom correspondence should be addressed. Tel.: 81-3-5449-5320; Fax: 81-3-5449-5420; E-mail: tinoue@ims.u-tokyo.ac.jp.

[1] The abbreviations used are: IP_3, inositol 1,4,5-trisphosphate; IP_3R, inositol 1,4,5-trisphosphate receptor; ER, endoplasmic reticulum; IICR, IP_3-induced Ca^{2-} release; IP_3R1, inositol 1,4,5-trisphosphate receptor type 1; AMPA, α-amino-3-hydroxy-5-methyl-4-isoxazole-propionic acid; AMPAR, AMPA type glutamate receptor; FRAP, fluorescence recovery after photobleaching; SERCA, sarcoplasmic/endoplasmic reticulum calcium-ATPase; IP_3R3, inositol 1,4,5-trisphosphate receptor type 3; GFP, green fluorescent protein; mRFP, monomeric red fluorescent protein; CTD, C-terminal domain; CTT, C-terminal cytoplasmic tail; HA, hemagglutinin.

protein 4.1N, which binds to the C terminus of IP_3R1 (17), may play crucial roles in the actin-dependent regulation of IP_3R1 diffusion.

EXPERIMENTAL PROCEDURES

DNA Constructions—All of the plasmids were propagated in the *Escherichia coli* strain HB101. All PCR products were verified by nucleotide sequencing using an ABI PRISM 377 automated sequencer (Applied Biosystems, Foster City, CA). The constructions of GFP-tagged sarcoplasmic/endoplasmic reticulum calcium-ATPase 2a (GFP-SERCA2a) (18), GFP-tagged IP_3R1 (GFP-IP_3R1), GFP-IP_3R1-ΔCTT14aa, and HA-4.1N-FL (17) were described previously. GFP-tagged IP_3R3 (GFP-IP_3R3)[2] was generated using cDNA clones of mouse IP_3R3 and a cDNA fragment coding enhanced green fluorescent protein. GFP-H2L[c]in (19) was kindly provided by Dr. Edidin (The Johns Hopkins University, Baltimore, MD). DsRed2–4.1N-FL and DsRed2–4.1N-CTD were generated by replacing a Venus fragment, a variant of yellow fluorescent protein (20), in pcDNA3-Venus-4.1N-FL and pcDNA3-Venus-4.1N-CTD (17) with DsRed2 (BD Biosciences, San Jose, CA), a gene encoding a red fluorescent protein.

A monomeric red fluorescent protein (mRFP) expression plasmid (pcDNA3.1/Zeo−-mRFP) was generated by inserting a fragment encoding mRFP (21), which was kindly provided by Dr. Tsien (University of California, San Diego, CA), into the EcoRI-BamHI site of pcDNA3.1/Zeo+ (Invitrogen). mRFP-CTT14aa, namely mRFP-fused with the C-terminal 14 residues of IP_3R1, was generated by inserting a synthesized DNA fragment corresponding to amino acids 2736–2749 of mouse IP_3R1 into the EcoRI-XhoI site of pcDNA3.1/Zeo+-mRFP.

To construct a chimeric cDNA GFP-IP_3R3-CTT14aa, we synthesized primers 1 (5′-CATGAGCCGGGGACATCCTCCTCAC-3′), 2 (5′-CAACAACGCACAGAATCTAGC-3′), 3 (5′-GACAAGATGGACTGTGTCTC-3′), 4 (5′-GAGGATGTCCCCGGTCATGCAGTTC-3′), and 5 (5′-TGCTTCATCTCTGGCCTGGAG-3′). First, cDNA sequences encoding amino acids 2735–2740 of IP_3R1 and amino acids 2666–2670 of IP_3R3 were amplified by PCR with primer set 1 and 2 and primer set 3 and 4, and pBlueBac4.5-C1[2] and pcDNA3.1/Zeo+-EC3 as templates, respectively. The PCR products were mixed, denatured, annealed, and reamplified using primer set 2 and 5 to create a chimeric sequence. The chimeric product and the original pcDNA3.1/Zeo+-EC3 were both digested with SacII and XbaI and ligated together to obtain the full-length chimera GFP-IP_3R3-CTT14aa in pcDNA3.1/Zeo+.

Primary Culture and Transfection of Hippocampal Neurons—Primary cultures of hippocampal neurons were prepared from the hippocampi of 1-day-old Wistar rats, as described previously (16). Briefly, dissociated cells were plated on poly-L-lysine (Nacalai Tesque, Kyoto, Japan)-coated coverslips at a density of 3.2×10^4 cells/cm^2 and cultured in Neurobasal Medium (Invitrogen) supplemented with 2.5 mM L-glutamine (Nacalai Tesque), 2.5% (v/v) B-27 (Invitrogen), and antibiotics (250 units/ml penicillin and 250 μg/ml streptomycin).

The cultures were transfected with 10 μg of the DNAs, usually on days 4–5 *in vitro*, using a standard calcium phosphate method (22). The transfected cells were used for cytochemistry or imaging experiments 2–3 days after the transfection.

Time Lapse Imaging and Photobleaching Experiments—For the time lapse imaging experiments, the culture medium was supplemented with 20 mM HEPES (pH 7.3). Fluorescence images of the cells were taken under a confocal scanning microscope (FV-300; Olympus, Tokyo, Japan) attached to an inverted microscope (IX70; Olympus) with a 60× objective (NA 1.4 or 1.45, oil immersion, UplanApo; Olympus). The temperature was maintained at 37 °C using a heating chamber that surrounded the microscope stage. The GFP signal was excited at 488 nm, and emission was detected through a 510–550-nm bandpass filter. The FRAP technique was carried out as follows. An image was taken before the photobleaching (Before) with a low laser power (6% of full power) and a scanning area (66 × 88 μm), and the center area of the field of view was bleached out with continuous high power (100%) laser scanning with a scanning area (20 × 27 μm) for 40 s. The laser power and scanning area were then returned to the initial settings, and the fluorescence recovery into the photobleached area was monitored every 5 s for 5 min. The images were stored at a resolution of 600 × 800 pixels. The images shown in Figs. 1 (*A* and *B*) and 3*A* were processed after digital smoothing to reduce the noise level. The smoothing filter is implemented using 3 × 3 spatial convolutions, where the value of each pixel in the selection is replaced with the weighted average of its 3 × 3 neighborhood. Center pixels are weighted 4-fold more than surrounding pixels.

Estimation of the Effective Diffusion Constant (D_{eff})—In a previous study (18), we quantified the movement of ER proteins as the apparent velocity of the fluorescence recovery after photobleaching, which was effective for comparing the speed of protein diffusion under the same experimental conditions, but we could not compare them to the diffusion constants of other proteins reported in the literature. To solve this issue, we adopted a different approach that enabled direct estimation of the effective diffusion constants (D_{eff}) of ER proteins from the FRAP results. We adopted a theory described by Siggia *et al.* (23) in which the movement of proteins on the ER membrane is simulated by diffusion in random media.

Throughout this study, we considered the ER networks in neuronal dendrites to be one-dimensional along dendrites, because the thicknesses of the target dendrites were much thinner than the photobleached length. We thus simulated the axial movement of the fluorescent signals as one-dimensional diffusion using the model proposed by Siggia *et al.* (23). To convert the basic data set, which consisted of a prebleach image and a series of postbleach images of 12-bit precision, to a series of one-dimensional data sets, the following arrangements were carried out. During the experiments, the cells were placed so that the dendrites lay horizontally in the image frame. During the analysis, the image was rotated if necessary to ensure that the target dendrite was horizontal (parallel to the x axis; Fig. 1*A*). A sufficiently large rectangular strip was then selected, including the bleached region of the dendrite, with its long axis in the x direction, and further analysis was performed within this rectangle (Fig. 1*B*). The fluorescence intensity data in the rectangle was compressed in the y direction by averaging to create one-dimensional data sets ("line compress"), which were stacked to create a two-dimensional data set (the second axis represents time; Fig. 1*C*). To reduce noise, four contiguous pixels along the x axis were further averaged to make a "binned" pixel strip of N pixels ($F_x(t)$).

The background fluorescence, which included the offset of the analog/digital conversion added in reading the photomultiplier output of the confocal scanner, was obtained by averaging the pixel intensities over a region of the image that did not contain any cell structures. The time constant of the photobleaching during the acquisition of the postbleach images was estimated by fitting the fluorescence intensity decay of the entire cell area to an exponential function.

We calculated the theoretical time course using Equations 1 and 2, which are derived from Equations 11 and 12, respectively, of Siggia *et al.* (23) by slight modifications to introduce the photobleach correction,

$$j_{i+1/2} = 0.5D_{eff}e^{-T/\tau}(\bar{\rho}_{i+1} + \bar{\rho}_i)((\rho/\bar{\rho})_{i+1} - (\rho/\bar{\rho})_i) \quad \text{(Eq. 1)}$$

$$\rho_i(t + \delta) = \rho_i(t) + \delta(j_{i+1/2} - j_{i-1/2}) \quad \text{(Eq. 2)}$$

where T is the time lapse interval, τ is the photobleach time constant, $j_x(t)$ is the current of the fluorescence, and $\rho_x(t)$ is the fluorescence density to which the raw data $F_x(t)$ was fitted. $\bar{\rho}$ corresponds to the initial fluorescence distribution calculated from the prebleach image. The actual pixel values obtained in experiments were used as a boundary condition ($F_0(t)$ and $F_{N-1}(t)$) for every time step, which effectively canceled the fluorescent decrease of the surrounding nonbleached areas during the photobleaching. We calculated $\rho_x(t)$ recursively with different values of the D_{eff} and determined the value that best fitted the real data $F_x(t)$. All of the analyses were performed using custom-made software (TI Workbench) running on a Macintosh computer. We have reported the existence of vesicular ERs, which are transported along dendrites, in addition to the reticular ER structure in hippocampal neurons (16). However, the total fluorescence signal of reticular ER was about 700-fold larger than that of vesicular ERs in dendrites (data not shown); we assumed that the effect of signal arising from the vesicular ER was negligible in this study. The data were expressed as the means ± S.D. Statistical analysis was performed using StatView (Abacus Concepts, Berkeley, CA). A comparison between the two groups was performed by an unpaired t test. Differences with p values less than 0.05 were considered to be statistically significant.

Drug Preparation and Immunocytochemistry—Stock solutions of latrunculin A (1 mg/ml; Invitrogen), jasplakinolide (1 mM; Invitrogen), and nocodazole (10 mg/ml; Sigma-Aldrich) were prepared in dimethyl sulfoxide and stored at −20 °C. The final concentrations of latrunculin A, jasplakinolide, and nocodazole in the culture medium were 1 μg/ml, 10 μM, and 30 μg/ml, respectively. To apply the drugs to the cells, a certain quantity of medium containing twice the final concentrations of the drugs was added to an equal volume of the culture medium. Cultured neurons were incubated with latrunculin A and nocodazole for 1 h each or with jasplakinolide for 3 h at 37 °C in 5% CO_2.

[2] M. Iwai, Y. Tateishi, M. Hattori, A. Mizutani, A. Futatsugi, T. Inoue, T. Furuichi, T. Michikawa, and K. Mikoshiba, unpublished data.

To confirm that the cytoskeleton was disrupted or polymerized, fixed cells were stained with Alexa 594-conjugated phalloidin (Invitrogen) or an anti-tubulin antibody (Lab Vision, Fremont, CA). The cells were fixed with 4% formaldehyde in phosphate-buffered saline for 10 min. After permeabilization with 0.1% Triton X-100 in phosphate-buffered saline for 10 min and blocking with 5% skim milk in phosphate-buffered saline, the cells were incubated with the anti-tubulin antibody (1:500 dilution) or Alexa 594-conjugated phalloidin (1:40 dilution). Alexa 488-conjugated IgGs (Invitrogen) were used as the secondary antibody for the anti-tubulin antibody.

Co-immunoprecipitation and Immunoblotting—COS-7 cells were maintained in Dulbecco's modified Eagle's medium (Nacalai Tesque) supplemented with 10% heat-inactivated fetal bovine serum. Five μg DNA/10-cm diameter culture dish was transfected using TransIT transfection regents (Mirus, Madison, WI) according to the manufacturer's protocol. Transfected COS-7 cells were harvested 1 day after transfection, and the lysates were prepared as previously described (24). The cell lysates were centrifuged at 10,000 $\times$ *g* for 30 min at 4 °C, and the supernatants were used for immunoprecipitation. The lysates were preincubated with 5–10 μg of an anti-HA mouse monoclonal antibody (clone 12CA5; Roche Applied Science) or an anti-mouse IgG antibody (Sigma) for 1 h at 4 °C and then incubated with 30 μl of protein G-Sepharose (Amersham Biosciences) for 2–3 h at 4 °C. The complexes were then centrifuged and washed with buffer three times. The proteins were eluted by boiling in 1× SDS-PAGE sample buffer for 3 min and separated by SDS-PAGE. The proteins were transferred to polyvinylidene difluoride membranes (Millipore), and the membranes were probed with an anti- enhanced green fluorescent protein antibody (Santa Cruz, Santa Cruz, CA) and an anti-HA antibody (Zymed Laboratories Inc., South San Francisco, CA).

RESULTS

Movement of GFP-tagged ER Membrane Proteins in Dendrites—Cultured rat hippocampal neurons were transfected with GFP-tagged IP$_3$R1 (GFP-IP$_3$R1) or GFP-tagged SERCA2a (GFP-SERCA2a) to observe the dynamics of ER membrane proteins in dendrites (Fig. 1*A*). A segment of each dendrite was photobleached, and the recovery of fluorescence into the bleached area was measured. As shown in Fig. 1*B*, both GFP-IP$_3$R1 and GFP-SERCA2a gradually migrated into the photobleached area from both ends. The movements of these proteins were also visualized by constructing "compressed images" from time lapse image stacks (Fig. 1*C*; refer to Experimental Procedures). This apparent diffusive nature allowed us to measure the effective diffusion constant (D_{eff}) by fitting to a diffusion model, which was specialized for modeling diffusion in a straight tubular structure, such as a dendrite (see "Experimental Procedures"). To examine the validity of this model in neuronal dendrites, we measured the D_{eff} of a smaller ER protein, GFP-tagged mouse major histocompatibility complex class I H2L^d (GFP-H2L^{d}in) (19) in dendrites and compared this D_{eff} with that reported for the same protein in non-neuronal cells. The diffusion coefficient of GFP-H2L^{d}in has been reported to be ~0.40 μm^2/s in the absence of interaction with the transporter associated with antigen processing 1 complex in L or EE2H cell lines (19). In dendrites of hippocampal neurons, in which no mRNA for transporter associated with antigen processing 1 is detected (26), the D_{eff} of GFP-H2L^{d}in was 0.46 ± 0.13 μm^2/s (n = 25). The similarity between the D_{eff} values shows that our model adequately calculates the diffusion constants in dendrites. Interestingly, the D_{eff} of GFP-IP$_3$R1 (0.26 ± 0.10 μm^2/s, n = 18) was significantly smaller than those of GFP-SERCA2a (0.47 ± 0.13 μm^2/s, n = 11) and GFP-H2L^{d}in (0.46 ± 0.13 μm^2/s, n = 25) (Fig. 2).

GFP-IP$_3$R1 Diffusion Is Sensitive to Actin Filament-destabilizing or -stabilizing Drugs—The diffusion of plasma membrane proteins is regulated by the cytoskeleton, especially actin filaments (27, 28). We hypothesized that the slow diffusion of IP$_3$R1 was caused by an interaction with the cytoskeleton and tested this possibility by disturbing microtubules and actin filaments pharmacologically. Nocodazole (30 μg/ml) was used to disrupt microtubules, and latrunculin A (1 μg/ml) and jasplakinolide (10 μM) were used to disrupt and stabilize actin filaments, respectively. The effectiveness of the treatments with these compounds was confirmed by cytochemistry in cultured rat hippocampal neurons. After treatment with nocodazole, anti-tubulin antibody staining in neurons was reduced

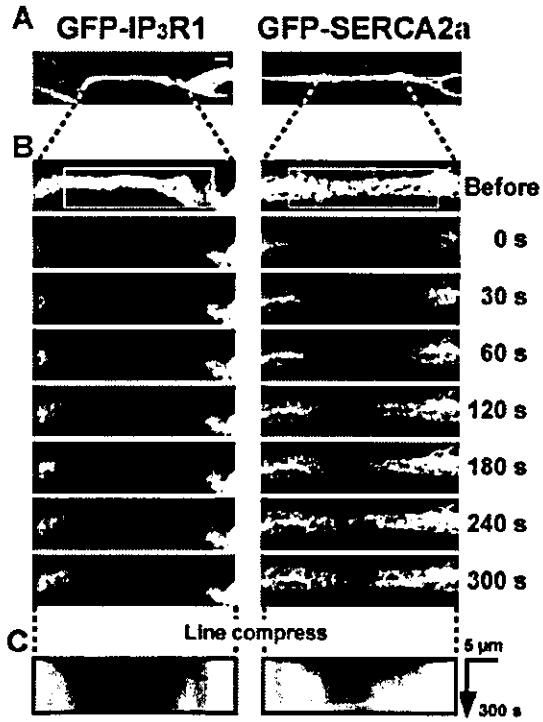

FIG. 1. **FRAP studies in dendrites of cultured hippocampal neurons expressing GFP-IP$_3$R1 and GFP-SERCA2a.** *A*, fluorescence images of neurons transfected with GFP-IP$_3$R1 and GFP-SERCA2a before FRAP. *Scale bar*, 5 μm. *B*, time lapse fluorescence images during FRAP. *Before*, higher magnification of the same images in *A*. The areas indicated by *white boxes* were photobleached and recovering fluorescence was recorded every 5 s. The images shown are picked out from the time lapse image stack. The amount of time after the termination of the photobleach is indicated. *C*, line-compressed images of fluorescence recovery were constructed from the time lapse image stacks (see "Experimental Procedures").

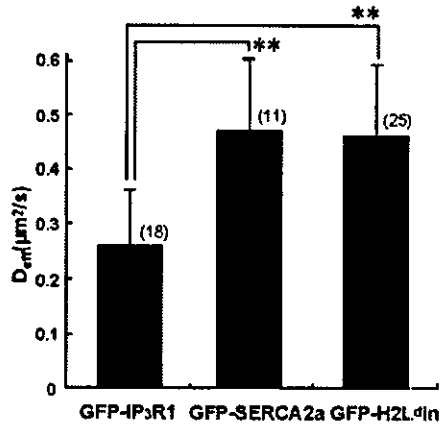

FIG. 2. **The D_{eff} of GFP-IP$_3$R1 is smaller than those of GFP-SERCA2a and GFP-H2L^{d}in.** Average effective diffusion constants (D_{eff}) of GFP-IP$_3$R1, GFP-SERCA2a and GFP-H2L^{d}in in dendrites. Note that the D_{eff} of GFP-IP$_3$R1 is 1.8-fold smaller than those of GFP-SERCA2a and GFP-H2L^{d}in. The data represent the means ± S.D. **, $p < 0.01$. The *numbers* in *parentheses* indicate the numbers of neurons examined.

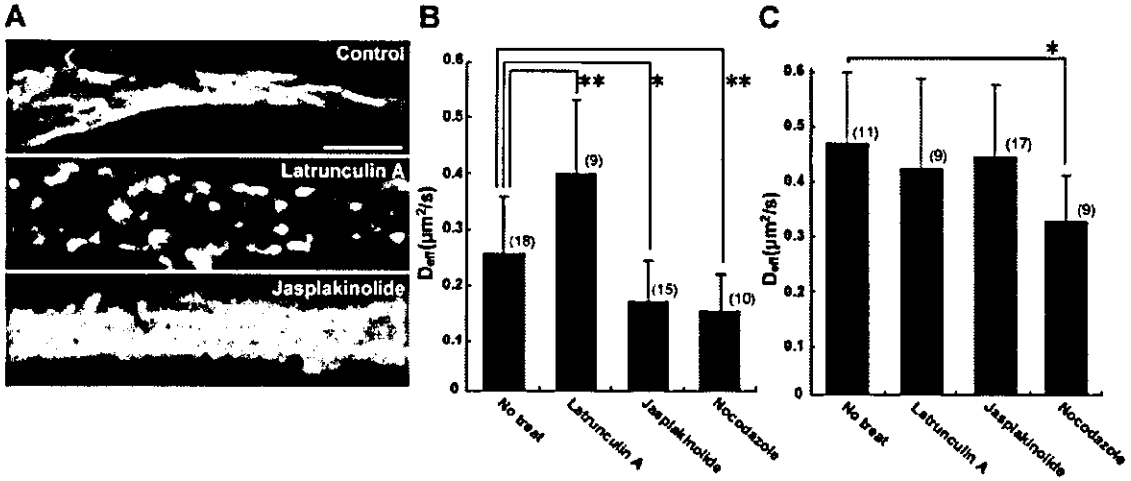

FIG. 3. **The D_{eff} of GFP-IP_3R1 is dependent on actin filaments, whereas that of GFP-SERCA2a is not.** *A*, effects of latrunculin A and jasplakinolide treatment on actin cytoskeleton. Fluorescence images of the dendrite of neurons stained with Alexa 594-conjugated phalloidin. *Scale bar*, 5 μm. *B* and *C*, the D_{eff} of GFP-IP_3R1 (*B*) and GFP-SERCA2a (*C*) without or with latrunculin A, jasplakinolide, and nocodazole treatments. Note that the D_{eff} of GFP-IP_3R1 is altered in the presence of the drugs that affect the actin filaments (latrunculin A and jasplakinolide), whereas that of GFP-SERCA2a is not. Treatment with nocodazole, which destabilizes microtubules, decreases the D_{eff} of GFP-IP_3R1 and GFP-SERCA2a. The data represent the means ± S.D. *, $p < 0.05$; **, $p < 0.01$. The *numbers* in *parentheses* indicate the numbers of neurons examined. The D_{eff} of GFP-IP_3R1 and GFP-SERCA2a for *No treat* are the same data shown in Fig. 2.

(data not shown). Latrunculin A reduced the density of actin filaments, whereas jasplakinolide turned individual bundles of actin filaments thick and dense (Fig. 3*A*). Treatment with nocodazole decreased the D_{eff} of GFP-IP_3R1 and GFP-SERCA2a to 0.16 ± 0.06 μm²/s (n = 10) and 0.33 ± 0.08 μm²/s (n = 9), respectively (Fig. 3, *B* and *C*), indicating that the integrity of microtubules is an important determinant for the diffusion rate of ER proteins. To our surprise, manipulation of actin filaments only affected the diffusion rate of IP_3R1. The D_{eff} of GFP-IP_3R1 was increased by latrunculin A treatment and decreased by jasplakinolide treatment to 0.40 ± 0.13 μm²/s (n = 9) and 0.18 ± 0.07 μm²/s (n = 15), respectively (Fig. 3*B*). However, the D_{eff} of GFP-SERCA2a remained unchanged after treatments with latrunculin A and jasplakinolide at 0.43 ± 0.16 μm²/s (n = 9) and 0.45 ± 0.13 μm²/s (n = 17), respectively (Fig. 3*C*). These data suggest that the movement of GFP-IP_3R1 is negatively regulated through actin filaments, whereas that of GFP-SERCA2a is not. We decided to concentrate on investigating the actin-mediated molecular mechanisms that specifically regulate the diffusion of IP_3R1.

4.1N Binding Regulates the Diffusion Rate of GFP-IP_3R1—We recently found that protein 4.1N, an actin-spectrin-binding protein, binds to the C-terminal cytoplasmic tail of IP_3R1 via its C-terminal domain, and regulates IP_3R1 localization in the Madin-Darby canine kidney cell line (17). Because 4.1N is expressed in central nervous system neurons, including those in the hippocampus, and its expression has also been shown in cultured hippocampal neurons (29), we therefore considered 4.1N to be a good candidate for the actin-mediated control of IP_3R1 diffusion. To test this possibility, we investigated the effects of DsRed2 (a red fluorescent protein)-tagged 4.1N fusion proteins on the D_{eff} of GFP-IP_3R1. Overexpression of DsRed2-tagged full-length 4.1N (DsRed2–4.1N-FL) or DsRed2 alone had little effect on the D_{eff} of GFP-IP_3R1 (0.25 ± 0.09 μm²/s, n = 21) and (0.24 ± 0.13 μm²/s, n = 11), respectively (Fig. 4). Next, we analyzed the effect of overexpression of a dominant-negative form of 4.1N, namely a C-terminal domain of 4.1N (4.1N-CTD) that lacks the actin-spectrin-binding domain (17), on the D_{eff} of GFP-IP_3R1. Interestingly, overexpression of the dominant-negative 4.1N increased the D_{eff} of GFP-IP_3R1 to 0.41 ± 0.15 μm²/s (n = 11), which was similar to

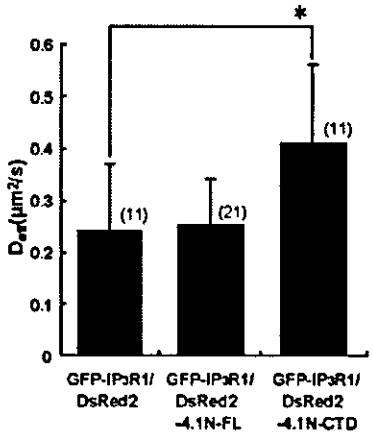

FIG. 4. **The 4.1N-CTD fragment increases the D_{eff} of GFP-IP_3R1.** The D_{eff} of GFP-IP_3R1 under co-expression with DsRed2, DsRed2–4.1N-FL, or DsRed2–4.1N-CTD. The D_{eff} of GFP-IP_3R1 co-expressed with DsRed2–4.1N-FL is not significantly different from that with DsRed2, whereas that after co-expression with DsRed2–4.1N-CTD increases. The data represent the means ± S.D. *, $p < 0.05$. The *numbers* in *parentheses* indicate the numbers of neurons examined.

the D_{eff} after latrunculin A treatment (Fig. 4). On the other hand, the D_{eff} of GFP-SERCA2a remained unchanged, showing no apparent side effects of the overexpression of DsRed2–4.1N-CTD (Table I). These results suggest that DsRed2–4.1N-CTD disrupted the interaction of GFP-IP_3R1 with endogenous 4.1N and support our idea that actin filaments affect the diffusion rate of GFP-IP_3R1 through 4.1N.

GFP-IP_3R1 Diffusion Is Regulated by the CTT14aa Site—The 4.1N-binding region of IP_3R1 was identified as the C-terminal 14 amino acids of the cytoplasmic tail: CTT14aa (17). To confirm whether the 4.1N interaction with CTT14aa was responsible for the negative regulation of GFP-IP_3R1 diffusion, we observed the diffusion of GFP-tagged IP_3R3 (GFP-IP_3R3), one of the isoforms of IP_3Rs that lacks a segment corresponding to CTT14aa (Fig. 5*A*). We confirmed that GFP-IP_3R3 did not bind to 4.1N by immunoprecipitation (Fig. 5*B*). The D_{eff} of GFP-IP_3R3 (0.45 ± 0.13 μm²/s, n = 20) was significantly larger

TABLE I
Effective diffusion constants (D_{eff}) of various proteins
The values shown are the means ± S.D.

Proteins	D_{eff}	Number of cells
	$\mu m_2/s$	
GFP-IP$_3$R1/mRFP	0.22 ± 0.11	11
GFP-SERCA2a/DsRed2–4.1N CTD	0.49 ± 0.16	9
GFP-SERCA2a/DsRed2	0.46 ± 0.19	7
GFP-SERCA2a/mRFP-CTT14aa	0.49 ± 0.10	10

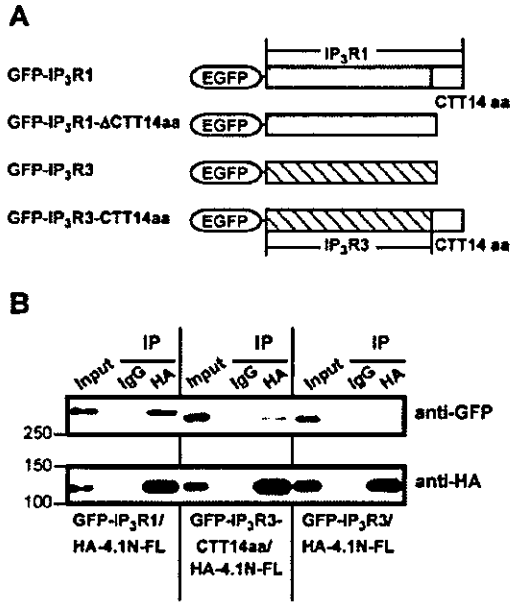

FIG. 5. **Association between IP$_3$R3-CTT14aa and 4.1N *in vitro*.** *A*, schematic representation of the structures of GFP-IP$_3$R1, GFP-IP$_3$R1-ΔCTT14aa, GFP-IP$_3$R3, and GFP-IP$_3$R3-CTT14aa. *B*, HA-4.1N-FL was transiently transfected to COS-7 cells with GFP-IP$_3$R1, GFP-IP$_3$R3-CTT14aa, or GFP-IP$_3$R3, and the cell lysates were immunoprecipitated (*IP*) with an anti-HA antibody or control IgG. The input and immunoprecipitated proteins were subjected to SDS-PAGE followed by Western blotting with anti-GFP and anti-HA antibodies. GFP-IP$_3$R1 and GFP-IP$_3$R3-CTT14aa bound to HA-4.1N-FL.

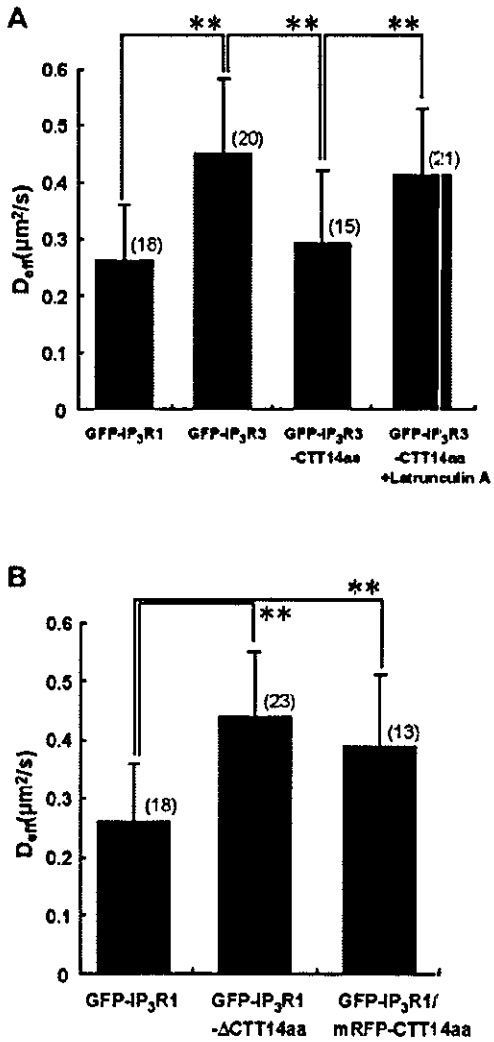

FIG. 6. **CTT14aa is involved in the regulation of GFP-IP$_3$R1 diffusion.** *A*, the D_{eff} of GFP-IP$_3$R3 and GFP-IP$_3$R3-CTT14aa and the D_{eff} of GFP-IP$_3$R3-CTT14aa treated with latrunculin A. Note that the D_{eff} of GFP-IP$_3$R3-CTT14aa is smaller than that of GFP-IP$_3$R3 and that it is increased by latrunculin A treatment. *B*, the D_{eff} of GFP-IP$_3$R1-ΔCTT14aa and GFP-IP$_3$R1 under co-expression with mRFP-CTT14aa, both of which are larger than that of GFP-IP$_3$R1. The data represent the means ± S.D. **, $p < 0.01$. The *numbers* in *parentheses* indicate the numbers of neurons examined. The D_{eff} of GFP-IP$_3$R1 in *A* and *B* are the same data shown in Fig. 2.

than that of GFP-IP$_3$R1 (Fig. 6*A*). On the other hand, the diffusion of GFP-IP$_3$R3-CTT14aa, GFP-IP$_3$R3 fused with CTT14aa at its C-terminal (Fig. 5*A*), showed properties similar to IP$_3$R1 rather than to IP$_3$R3. We confirmed the binding of GFP-IP$_3$R3-CTT14aa to 4.1N by immunoprecipitation (Fig. 5*B*). The D_{eff} of GFP-IP$_3$R3-CTT14aa in dendrites (0.29 ± 0.13 $\mu m^2/s$, $n = 15$) was close to that of GFP-IP$_3$R1 (Fig. 6*A*) and significantly smaller than that of GFP-IP$_3$R3 (Fig. 6*A*). Latrunculin A treatment increased the D_{eff} of GFP-IP$_3$R3-CTT14aa to 0.41 ± 0.12 $\mu m^2/s$ ($n = 21$), which was close to that of GFP-IP$_3$R3 (Fig. 6*A*). This result suggests that CTT14aa serves as a linker for the actin-mediated diffusion control of IP$_3$R1.

To further investigate whether CTT14aa was involved in the regulation of GFP-IP$_3$R1 diffusion through interaction with 4.1N, GFP-IP$_3$R1-ΔCTT14aa (GFP-tagged IP$_3$R1 lacking the last 14 amino acids, *i.e.* CTT14aa; Fig. 5*A*), which does not bind to 4.1N (17), was expressed in neurons. The D_{eff} of GFP-IP$_3$R1-ΔCTT14aa (0.44 ± 0.11 $\mu m^2/s$, $n = 23$) was significantly larger than that of GFP-IP$_3$R1 and close to those of GFP-IP$_3$R3 and GFP-SERCA2a (Fig. 6*B*). We then overexpressed a CTT14aa peptide, which is expected to compete with the GFP-IP$_3$R1 for the binding site in the endogenous 4.1N. mRFP-tagged CTT14aa significantly increased the diffusion constant of GFP-IP$_3$R1 (0.39 ± 0.12 $\mu m^2/s$, $n = 13$) while leaving the diffusion constant of GFP-SERCA2a unchanged (Fig. 6*B* and Table I). Overexpression of mRFP did not affect the D_{eff} of GFP-IP$_3$R1 (Table I). Taking all of the results together, we conclude that the last 14-amino acid segment of IP$_3$R1, CTT14aa, is involved in the actin-dependent regulation of the GFP-IP$_3$R1 diffusion rate by interaction with 4.1N (Fig. 7).

DISCUSSION

Nature of the IP$_3$R1 Diffusion—In the present study, we showed that ER membrane proteins IP$_3$R1, SERCA2a, and H2L^{d}in diffused on the reticular ER membrane in neuronal dendrites (Figs. 1 and 2). This is the first report describing the diffusion of ER membrane proteins and calculating their D_{eff} in neuronal dendrites. The D_{eff} of GFP-IP$_3$R1 (0.26 $\mu m^2/s$) was 1.8-fold smaller than those of GFP-SERCA2a and GFP-H2L^{d}in (0.47 and 0.46 $\mu m^2/s$, respectively; Fig. 2). This result shows heterogeneity in the diffusion rates of ER proteins. It has been proposed that the diffusion of proteins on biological membranes

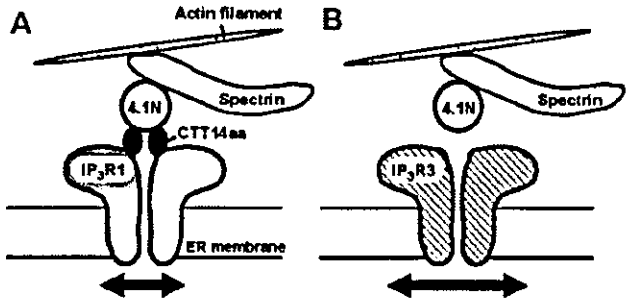

FIG. 7. **Schematic model of regulatory mechanism for IP$_3$R1 diffusion.** *A*, protein 4.1N binds spectrin-actin filaments and CTT14aa of IP$_3$R1. Therefore IP$_3$R1 does not diffuse freely. *B*, IP$_3$R3 does not bind to 4.1N. Therefore it is able to diffuse freely.

is dependent on the size of the transmembrane region of each protein (30), although this does not appear to be consistent with our results. The D_{eff} of GFP-IP$_3$R3, GFP-SERCA2a, and GFP-H2L^{d}in, which are expected to have transmembrane regions of different sizes, were quite similar (0.45–0.47 $\mu m^2/s$) (Figs. 2 and 6*A*). Moreover, the D_{eff} of GFP-IP$_3$R1 was smaller than that of GFP-IP$_3$R3 (Fig. 6*A*), despite the similarity in size of their transmembrane regions as well as of the whole molecules. Thus, we consider that the small D_{eff} of GFP-IP$_3$R1 compared with those of other ER proteins is not due to the difference in molecular size but rather to a negative regulatory mechanism specific for IP$_3$R1 diffusion.

We previously reported that the movement velocity of the GFP-tagged C-terminal half of IP$_3$R1, containing the transmembrane region, was similar to that of GFP-SERCA2a in the axons of chick dorsal root ganglion neurons (18). The discrepancy between this study and the previous one may arise from the difference in the cellular region studied (dendrites *versus* axons), the cell type, or the structure of the IP$_3$R1 used (full-length *versus* truncated form).

Regulatory Mechanism of the GFP-IP$_3$R1 Diffusion—The diffusion of plasma membrane proteins is regulated by the cytoskeleton, especially actin filaments (reviewed in Refs. 27 and 28). Actin filaments are also involved in the regulation of phospholipids diffusion in the plasma membrane (31). In this study, we have demonstrated an example of actin-mediated regulation of ER protein diffusion for the first time. It has been reported that the integrity of actin filaments affects IICR properties (32). The specific regulation of IP$_3$R1 diffusion by actin filaments found in the present study could be underlying such functional regulations of Ca^{2+} release by actin cytoskeleton in neurons.

The contribution of microtubules was almost the same for the diffusion of GFP-IP$_3$R1 and GFP-SERCA2a (Fig. 3, *B* and *C*). Because microtubules are known to be involved in the dynamics of the ER membrane, such as tubule branching, ring closure, and sliding (33, 34), the diffusion of GFP-IP$_3$R1 and GFP-SERCA2a may not be dependent on their direct interaction with microtubules but rather on changes in the dynamics of the ER membrane. Further studies are required to verify this hypothesis, and investigating the contribution of microtubules to the regulation of the dynamics of other ER proteins may be useful for addressing this issue.

In the present study, we focused on an actin filament-dependent regulatory mechanism for the diffusion of GFP-IP$_3$R1 through 4.1N (Figs. 4 and 6). Fig. 7 shows a schematic model of the regulation of IP$_3$R1 diffusion. Protein 4.1N that contains an actin-spectrin-binding domain was identified as a binding protein of the C-terminal 14 amino acids of IP$_3$R1 (17). Because other protein 4.1 homologues play critical roles in the mechanical stability of the plasma membrane, and 4.1N is also postulated to play such a role (29). Recently, 4.1N is also reported to play roles in the translocation or cell surface expression of receptor molecules. In polarized Madin-Darby canine kidney cells, 4.1N is required for IP$_3$R1 translocation to the basolateral membrane domain (17). In neurons, there is growing evidence suggesting that 4.1N is involved in the regulation of the surface expression of receptors and channels in the plasma membrane, such as D2 and D3 dopamine (35) and AMPA (24) receptors. In the latter case, cross-linking of AMPAR to actin filaments through 4.1N is postulated (24). These findings, together with the present results, indicate that 4.1N may regulate proteins on both the plasma membrane and the ER membrane in neurons. However, the present data do not mean that 4.1N is the only regulatory protein for IP$_3$R1 diffusion. Because numerous IP$_3$R1-binding proteins are known (36), including proteins that interact with actin filaments, *e.g.* ankyrin 2, β-spectrin, and α-fodrin (37), proteins other than 4.1N may also contribute to the regulation of IP$_3$R1 diffusion through linking to actin filaments. This study is the first step in elucidating the possibly complex regulatory mechanism of IP$_3$R1 diffusion.

Finally, we would like to speculate on the physiological roles for this regulatory mechanism of IP$_3$R1 diffusion. IP$_3$R1 is responsible for various neuronal activities, *e.g.* synaptic plasticity in postsynapse (6–8) and nerve growth in growth cones (5). Interestingly, actin filaments are enriched in the dendritic spines and growth cones where IICR from IP$_3$R1 is reported to be important for physiological functions (38–40). Heterogeneous distribution of some of the Ca^{2+}-handling ER proteins is considered to be important for generating spatially complex Ca^{2+} signal (12), and negative regulation of IP$_3$R1 diffusion by actin filaments may be involved in the spatial heterogeneity of IP$_3$R1, namely the spatial regulation of Ca^{2+} release that influences various neuronal activities such as synaptic plasticity and nerve growth, especially in neurons expressing 4.1N.

Acknowledgments—We are grateful to Dr. R. Tsien for the gift of mRFP and to Dr. M. Edidin for the gift of GFP-H2L^{d}in. We thank Dr. M. Hattori and Dr. T. Michikawa for valuable discussions and M. Iwai, Y. Tateishi, Dr. A. Mizutani, and N. Ogawa for technical assistance.

REFERENCES

1. Berridge, M. J. (1993) *Nature* **361**, 315–325
2. Furuichi, T., and Mikoshiba, K. (1995) *J. Neurochem.* **64**, 953–960
3. Matsumoto, M., Nakagawa, T., Inoue, T., Nagata, E., Tanaka, K., Takano, H., Minowa, O., Kuno, J., Sakakibara, S., Yamada, M., Yoneshima, H., Miyawaki, A., Fukuuchi, Y., Furuichi, T., Okano, H., Mikoshiba, K., and Noda, T. (1996) *Nature* **379**, 168–171
4. Street, V. A., Bosma, M. M., Demas, V. P., Regan, M. R., Lin, D. D., Robinson, L. C., Agnew, W. S., and Tempel, B. L. (1997) *J. Neurosci.* **17**, 635–645
5. Takei, K., Shin, R. M., Inoue, T., Kato, K., and Mikoshiba, K. (1998) *Science* **282**, 1705–1708
6. Fujii, S., Matsumoto, M., Igarashi, K., Kato, H., and Mikoshiba, K. (2000) *Learn. Mem.* **7**, 312–320
7. Nishiyama, M., Hong, K., Mikoshiba, K., Poo, M. M., and Kato, K. (2000) *Nature* **408**, 584–588
8. Inoue, T., Kato, K., Kohda, K., and Mikoshiba, K. (1998) *J. Neurosci.* **18**, 5366–5373
9. Finch, E. A., and Augustine, G. J. (1998) *Nature* **396**, 753–756
10. Takechi, H., Eilers, J., and Konnerth, A. (1998) *Nature* **396**, 757–760
11. Miyata, M., Finch, E. A., Khiroug, L., Hashimoto, K., Hayasaka, S., Oda, S. I., Inouye, M., Takagishi, Y., Augustine, G. J., and Kano, M. (2000) *Neuron* **28**, 233–244
12. Papp, S., Dziak, E., Michalak, M., and Opas, M. (2003) *J. Cell Biol.* **160**, 475–479
13. Carroll, R. C., Beattie, E. C., von Zastrow, M., and Malenka, R. C. (2001) *Nat. Rev. Neurosci.* **2**, 315–324
14. Borgdorff, A. J., and Choquet, D. (2002) *Nature* **417**, 649–653
15. Tardin, C., Cognet, L., Bats, C., Lounis, B., and Choquet, D. (2003) *EMBO J.* **22**, 4656–4665
16. Bannai, H., Inoue, T., Nakayama, T., Hattori, M., and Mikoshiba, K. (2004) *J. Cell Sci.* **117**, 163–175
17. Zhang, S., Mizutani, A., Hisatsune, C., Higo, T., Bannai, H., Nakayama, T., Hattori, M., and Mikoshiba, K. (2003) *J. Biol. Chem.* **278**, 4048–4056
18. Aihara, Y., Inoue, T., Tashiro, T., Okamoto, K., Komiya, Y., and Mikoshiba, K. (2001) *J. Neurosci. Res.* **65**, 236–246
19. Marguet, D., Spiliotis, E. T., Pentcheva, T., Lebowitz, M., Schneck, J., and Edidin, M. (1999) *Immunity* **11**, 231–240
20. Nagai, T., Ibata, K., Park, E. S., Kubota, M., Mikoshiba, K., and Miyawaki, A. (2002) *Nat. Biotechnol.* **20**, 87–90

21. Campbell, R. E., Tour, O., Palmer, A. E., Steinbach, P. A., Baird, G. S., Zacharias, D. A., and Tsien, R. Y. (2002) *Proc. Natl. Acad. Sci. U. S. A.* **99,** 7877–7882
22. Köhrmann, M., Haubensak, W., Hemraj, I., Kaether, C., Leßmann, V. J., and Kiebler, M. A. (1999) *J. Neurosci. Res.* **58,** 831–835
23. Siggia, E. D., Lippincott-Schwartz, J., and Bekiranov, S. (2000) *Biophys. J.* **79,** 1761–1770
24. Shen, L., Liang, F., Walensky, L. D., and Huganir, R. L. (2000) *J. Neurosci.* **20,** 7932–7940
25. Deleted in proof
26. Neumann, H., Schmidt, H., Cavalie, A., Jenne, D., and Wekerle, H. (1997) *J. Exp. Med.* **185,** 305–316
27. Choquet, D., and Triller, A. (2003) *Nat. Rev. Neurosci.* **4,** 251–265
28. Haggie, P. M., Stanton, B. A., and Verkman, A. S. (2004) *J. Biol. Chem.* **279,** 5494–5500
29. Walensky, L. D., Blackshaw, S., Liao, D., Watkins, C. C., Weier, H. U., Parra, M., Huganir, R. L., Conboy, J. G., Mohandas, N., and Snyder, S. H. (1999) *J. Neurosci.* **19,** 6457–6467
30. Saffman, P. G., and Delbrück, M. (1975) *Proc. Natl. Acad. Sci. U. S. A.* **72,** 3111–3113
31. Fujiwara, T., Ritchie, K., Murakoshi, H., Jacobson, K., and Kusumi, A. (2002) *J. Cell Biol.* **157,** 1071–1081
32. Wang, Y., Mattson, M. P., and Furukawa, K. (2002) *J. Neurochem.* **82,** 945–952
33. Lee. C., and Chen, L. B. (1988) *Cell* **54,** 37–46
34. Dabora, S. L., and Sheetz, M. P. (1988) *Cell* **54,** 27–35
35. Binda, A. V., Kabbani, N., Lin, R., and Levenson, R. (2002) *Mol. Pharmacol.* **62,** 507–513
36. Vermassen, E., Parys, J. B., and Mauger, J. P. (2004) *Biol. Cell* **96,** 3–17
37. Lencesova, L., O'Neill, A., Resneck, W. G., Bloch, R. J., and Blaustein, M. P. (2004) *J. Biol. Chem.* **279,** 2885–2893
38. Kaech, S., Parmar, H., Roelandse, M., Bornmann, C., and Matus, A. (2001) *Proc. Natl. Acad. Sci. U. S. A.* **98,** 7086–7092
39. Yamada, K. M., Spooner, B. S., and Wessells, N. K. (1971) *J. Cell Biol.* **49,** 614–635
40. Marsh, L., and Letourneau, P. C. (1984) *J. Cell Biol.* **99,** 2041–2047